

Local structure variations observed in orthoenstatite at high pressures

DONGZHOU ZHANG,^{1,*} JENNIFER M. JACKSON,¹ WOLFGANG STURHAHN,^{2,†} AND YUMING XIAO³

¹Seismological Laboratory, Division of Geological and Planetary Sciences, California Institute of Technology, 1200 E. California Boulevard, Pasadena, California 91125, U.S.A.

²Advanced Photon Source, Argonne National Laboratory, 9700 S. Cass Avenue, Argonne, Illinois 60439, U.S.A.

³HPCAT, Geophysical Laboratory, Carnegie Institution of Washington, Argonne, Illinois 60439, U.S.A.

ABSTRACT

The site-specific behavior of iron in an orthoenstatite-structured ⁵⁷Fe-enriched (M1)(M2)Si₂O₆ powdered sample was explored using synchrotron Mössbauer spectroscopy and diamond-anvil cells in two independent experiments at ambient temperature. In one experiment, NaCl was used as the pressure-transmitting medium (ambient pressure to 36 GPa), and in the other experiment, Ne surrounded the sample (4.1 to 26.8 GPa). The hyperfine parameters of the M1 and M2 sites at room pressure are in excellent agreement with previous literature values obtained using conventional Mössbauer spectroscopy and yield (Mg_{0.980}Fe_{0.020(5)})(Mg_{0.760}Fe_{0.240})Si₂O₆ as the chemical formula. Analyses of both data sets reveal a change in the trend or discontinuity in the hyperfine parameters around 10 GPa, indicative of a transformation in orthopyroxene. However, the detailed behaviors of the iron sites with pressure appear to depend on the local stress conditions provided by the different pressure media. Our observations may help explain the reported variations in structural transition behavior for orthopyroxenes at high pressures.

Keywords: Orthoenstatite, pyroxene, upper mantle, Mössbauer spectroscopy, nuclear resonant scattering

INTRODUCTION

The pyroxene group is an abundant mineralogical component in the Earth's top 400 km silicate shell and exists in the Earth in two major forms: orthopyroxene (Opx) and clinopyroxene. The common space group for Opx is *Pbca*, although experiments and theoretical simulations show the possibility of other forms, such as phases with space group *Pbcn*, *Cmca*, *Ibca*, or *P2₁ca*. (Yang and Ghose 1995; Jackson et al. 2004; Jahn 2008). Clinopyroxene (Cpx) can be further divided into low-pressure clinopyroxene (LP-Cpx, with space group *P2₁/c*) and the non-quenchable high-pressure clinopyroxene (HP-Cpx, with space group *C2/c*). Although some of these symmetries of Ca-poor pyroxene have been demonstrated in both laboratory and natural occurrences, Opx is one of the most abundant natural forms in the pyroxene group. Opx comprises anywhere from 5 to 40% by volume of rocks in the Earth's crust and upper mantle (e.g., Ringwood 1977; Anderson 2007). The structural transitions observed in pyroxenes at elevated pressures and temperatures have been thought to provide explanations of geophysical observations in the upper mantle, such as the "X-discontinuity" at approximately 240 to 340 km depth (8 to 11 GPa and ~1350 to 1450 °C) (Woodland 1998; Akashi et al. 2009) and low-velocity regions (Jackson et al. 2004; Reynard et al. 2010). However, seismological studies indicate that the depth of the "X-discontinuity" cannot be explained by a single Clapeyron slope (Deuss and Woodhouse 2002), and

several studies on Opx at high pressures have yielded different results regarding micro- and macroscopic details of the transition. In the iron-rich end-member, Fe₂Si₂O₆ ferrosilite, a *Pbca* to *C2/c* transition was observed to occur at 4.2 GPa and 300 K (Hugh-Jones et al. 1996). In other iron-rich Ca-poor pyroxenes, *Pbca* is also thought to transform into *C2/c* at high pressures (Hugh-Jones et al. 1994, 1996; Woodland and Angel 1997; Woodland 1998). In Mg-rich orthopyroxenes or orthoenstatites (Oen), the observations have been much more diverse. A Raman spectroscopy study on orthoenstatite Mg₂Si₂O₆ showed that a transition occurs at 9 GPa and 300 K and suggested that the new Raman pattern was consistent with a transition to *C2/c* (Hugh-Jones et al. 1997). Results on Mg₂Si₂O₆ using X-ray diffraction (Kung et al. 2004; Lin et al. 2005), ultrasonics (Kung et al. 2004, 2006), and Raman spectroscopy (Lin 2003; Lin et al. 2005) claim the observed high-pressure behavior in Mg₂Si₂O₆ is not consistent with a structural transition to *C2/c*, however the symmetry of the high-pressure phase could not be unambiguously determined. Recent molecular dynamics simulations and first-principles electronic structure calculations suggest that, at room temperature, *Pbca*-structured Mg₂Si₂O₆ may produce metastable displacive transitions to *P2₁ca* (at ~9 GPa) and *Pbca* at *P* > 20 GPa (Jahn 2008). These symmetries, however, have not been experimentally identified. Due to the relative abundance of Opx in the upper mantle and its potential to explain geophysical observations, a better understanding of its high-pressure behavior is needed.

Investigations on the pressure dependences of the site-specific behavior of Fe²⁺ cations in pyroxenes can provide insight to the nature of its phase transitions and can be accurately attained using Mössbauer spectroscopy. Conventional Mössbauer spectroscopy

* E-mail: dzzhang@caltech.edu

† Present address: Jet Propulsion Laboratory, 4800 Oak Grove Dr., Pasadena, CA 91109, U.S.A.

determines the hyperfine parameters and has been applied to understand pyroxenes under ambient-pressure conditions (e.g., Domeneghetti and Steffen 1992; Pasternak et al. 1992; Dyar et al. 2007; Klima et al. 2007; Jackson et al. 2009). Due in part to the large sample volumes required, limited photon flux and long measuring times, only one high-pressure study was carried out on iron-bearing pyroxenes using conventional Mössbauer spectroscopy (McCammon and Tennant 1996). In this particular study, the pressure response of iron's hyperfine parameters in $\text{Fe}_2\text{Si}_2\text{O}_6$ clinoferrosilite ($P2_1/c$) was measured to 4 GPa (McCammon and Tennant 1996). A structural transition to $C2/c$ was concluded based on the observation of a step-like discontinuity of the hyperfine parameters between 1.33 and 1.74 GPa, pressures consistent with a structural transition observed in a previous X-ray diffraction study on $\text{Fe}_2\text{Si}_2\text{O}_6$ clinoferrosilite (Hugh-Jones et al. 1994). Synchrotron Mössbauer spectroscopy (SMS) provides hyperfine parameters similar to conventional Mössbauer spectroscopy, but eliminates the ^{57}Co source broadening. The high photon brilliance and the high resolution from the third-generation synchrotron radiation significantly reduces the data collecting times, the required amount of sample containing the Mössbauer isotope, and pressure gradients in the measured data, making high-quality high-pressure measurements of iron-bearing samples possible (e.g., Sturhahn 2004; Sturhahn and Jackson 2007). For example, high-pressure SMS measurements have been performed on silicates, such as clinopyroxene-structured $\text{CaFeSi}_2\text{O}_6$ hedenbergite (Zhang et al. 1999) and more iron-dilute silicates (Jackson et al. 2005; Li et al. 2006; Lin et al. 2008; McCammon et al. 2008; Grocholski et al. 2009; Catalli et al. 2010). In this study, we carried out high-pressure SMS studies on $(\text{Mg},^{57}\text{Fe})_2\text{Si}_2\text{O}_6$ with space group $Pbca$ as the initial phase. By using NaCl and Ne as different pressure-media in two independent experiments, we also assessed the influence of pressure media on iron's local site behavior.

EXPERIMENTAL PROCEDURES

Sample preparation

Powdered samples of orthoenstatite-structured $(\text{Mg},^{57}\text{Fe}_{1-x})_2\text{Si}_2\text{O}_6$ with $x = 0.87$ (En87) were prepared as $\sim 25 \mu\text{m}$ thick pellets for high-pressure synchrotron Mössbauer spectroscopy experiments. The powdered samples in this experiment were taken from the same run that was used in a nuclear resonant scattering study at ambient conditions (Jackson et al. 2009). Two symmetric piston-cylinder diamond-anvil cells (DAC) were loaded with En87 pellets for high-pressure measurements. For each cell, two Type-I diamonds with culets $300 \mu\text{m}$ in diameter were mounted and aligned to form the anvil. Rhenium gaskets were pre-indented to $\sim 50 \mu\text{m}$ thickness, and a $100 \mu\text{m}$ diameter hole was drilled in the center of the pre-indentation using an electrical discharge machine. One cell was loaded with the En87 sample and dehydrated NaCl as the pressure-transmitting medium (hereafter referred to as En87-NaCl). A second cell was prepared with En87 and Ne as gas-loaded (Rivers et al. 2008) as the pressure-transmitting medium (hereafter referred to as En87-Ne). In each cell, a few ruby spheres ($\sim 10 \mu\text{m}$ in diameter) were placed around the En87 pellet to determine the pressure in the sample chamber.

Synchrotron Mössbauer spectroscopy

Synchrotron Mössbauer spectroscopy (SMS) provides detailed information on the hyperfine structure of the ^{57}Fe cations in materials (e.g., Sturhahn 2004). The hyperfine interaction describes the splitting of nuclear energy levels as a result of the hyperfine coupling to atomic or molecular energy levels. The quantities observed, which are most relevant to the current study are isomer shift (IS), quadrupole splitting (QS), and the distribution of QS. The IS is proportional to the s-electron density at the nucleus, and hence is indirectly influenced by the d-electron population in the

valence shell via shielding effects. The IS thus provides information on the valence or oxidation state of the Fe cations and is always obtained in a relative sense. IS values are obtained by placing a reference absorber with known composition and thickness in the X-ray beam path near the sample. The QS is observed when an electric field of non-cubic symmetry exists around the nuclei. In general, two factors can contribute to the electric field gradient: an electron distribution in the valence shell and/or a nearby lattice environment with non-cubic symmetry. Thus, QS data yield information on local chemical environment and in an independent manner to the isomer shift. The distribution of QS has a similar effect as the full-width at half maximum of an absorption peak in conventional Mössbauer spectroscopy. However, SMS does not suffer "source related broadening," allowing one to probe the distribution of field gradients caused only by the sample. As the QS indicates the local chemical environment of each iron cation site, the distribution of QS thus shows the variation of the local chemical environment. When the site has abundant local structure variations, usually the corresponding distribution of the QS is large. As explained in previous literature, a single doublet with certain set of IS, QS, and distribution of QS in conventional Mössbauer spectroscopy produces a characteristic oscillation in the SMS time spectrum with a periodicity equal to $2h/\text{QS}$, where h is the Planck's constant (Zhang et al. 1999). This set of hyperfine parameters is referred as an iron site because it represents a specific polyhedral Fe-containing site in the sample. If there are additional sites present, the composition SMS time spectrum will be a coherent superposition of all oscillations, where the difference in IS corresponds to the relative phase difference between each oscillation component.

The SMS experiments on En87-NaCl and En87-Ne were performed at beamlines 3-ID-B and 16-ID-D, respectively at the APS. Experiments were carried out at ambient temperature. Specific details concerning the experimental setup have been explained previously (Sturhahn 2004). In our experiment, the prompt broadband X-ray beam from the synchrotron was filtered to 1 meV (in Sector 3-ID-B) and 2 meV (in Sector 16-ID-D) bandwidths using silicon multiple-crystal Bragg reflection monochromators. A Kirkpatrick-Baez mirror system was used to obtain a vertical \times horizontal focus spot size of $15 \times 10 \mu\text{m}^2$ at 3-ID-B and $\sim 40 \times 60 \mu\text{m}^2$ at 16-ID-D at the full-width at half maximum. The storage ring was operated in top-up mode with 24 bunches that were separated by 153 ns. An avalanche photo diode detector was placed 100 cm in the downstream direction of the X-ray focus spot to collect coherent elastic photons (the SMS signal). Accounting for detector and bunch separation related effects, we were able to observe nuclear resonant scattering in a time window of 20 to 125 ns following excitation. The isomer shift of the iron sites was determined by placing a ^{57}Fe -enriched stainless steel foil with a physical thickness of $0.5 \mu\text{m}$ in the X-ray beam path in the downstream direction of the sample. The SMS spectra were collected with and without stainless steel foil with collection times of ~ 30 min per spectrum. We carried out SMS measurements on En87-NaCl from ambient pressure up to 36 GPa with pressure intervals of 1–2 GPa at pressures lower than 20 GPa and pressure intervals of ~ 5 GPa at higher pressures. For En87-Ne, the pressure range was 4.1 to 26.8 GPa with pressure steps of ~ 1.5 GPa.

Pressure uncertainties

The pressure was determined offline using the characteristic fluorescence spectral shift of the rubies surrounding the sample (Mao et al. 1986). Spectra were collected on individual rubies surrounding the sample before and after each SMS measurement to document the pressure distribution within the sample chamber and any pressure drift during the SMS measurement. The full-width at half maximum (FWHM) of the R1 peak was also determined. These variables were used in our method to characterize the pressure uncertainty. We report such an uncertainty in the form of a standard deviation. We find that for all pressures investigated, the FWHM of the R1 peak is always larger for the cell loaded with NaCl as a pressure medium than the cell loaded with a Ne pressure medium. For example, the uncertainty in pressure for the cell using NaCl medium is 2.4 GPa at ~ 26 GPa, whereas the largest pressure uncertainty for the cell using Ne medium is only 0.9 GPa at ~ 27 GPa. The level of non-hydrostaticity of the pressure-transmitting media is the cause of the large pressure uncertainties at high pressures (e.g., You et al. 2009).

SMS DATA EVALUATION AND RESULTS

CONUSS with a Beam-Search algorithm

We used the CONUSS software package to evaluate the time spectra of SMS measurements (Sturhahn 2000). It optimizes hyperfine parameters such as IS, QS, distribution of QS, as well as other parameters such as weights of individual sites, thick-

ness, and scaling factor. In addition to a standard least-square algorithm guided by local parameter derivatives, we implemented a Beam-Search algorithm using random trials into CONUSS. This new procedure permitted us to explore a large parameter space and to avoid inconvenient parameter correlations during the search for a local minimum of the least-square sum. We were also able to exclude shallow local minima and reduce the potential for an erroneous identification of such minima as best fits. These complications often impede best-fit attempts using local parameter derivatives, and the Beam-Search algorithm reduced the needed real-time for fitting of the time spectra and increased the reliability of our results. We report the best-fit parameters obtained from this approach with uncertainties given at the 90% confidence level for the last reported significant digit (Tables 1 and 2). An error correlation matrix for the fitted parameters at ambient pressure is provided in Table 1b. The correlation matrix gives the normalized covariance between each pair of fitting parameters. Each element in the matrix shows the degree of correlation between the parameters in the row and column of that element (± 1 = completely correlated, 0 = independent). All the diagonal elements are 1, because each parameter is completely correlated with itself.

A well-defined effective thickness allows one to determine the hyperfine parameters within the accuracy of our reported results. The effective thickness, η ($\eta = \rho \sigma_{LM} D$; Zhang et al.

1999; Sturhahn 2004), of each sample was calculated prior to the experiments and determined from the CONUSS fitting procedure. The calculation included the Lamb-Mössbauer factor (or recoilless fraction) determined directly from nuclear resonant inelastic X-ray scattering on a sample from the same run charge ($f_{LM} = 0.73 \pm 0.02$, Jackson et al. 2009) and the initial sample loading thickness of $D = 23 \pm 0.02 \mu\text{m}$, producing $\eta = 9.7 \pm 0.6$. This value is in excellent agreement with the values determined from CONUSS ($\eta \approx 10$).

The IS values we report are referenced to α -iron to readily compare with commonly reported IS values from conventional Mössbauer spectroscopy. At ambient pressure, two iron sites are clearly distinguishable by their hyperfine fields, namely the M1 and M2 octahedral sites, consistent with crystal structural analysis of orthopyroxenes (Cameron and Papike 1981). Within the uncertainties, all the Fe sites in the studied En87 samples can be identified as Fe^{2+} . We note that only in the En87-NaCl data set it is possible to fit $\sim 3\%$ of the total iron as a Fe^{3+} -like site without increasing the χ^2 of the fits. As this site bears negligible weight to the spectra and does not improve the χ^2 , we exclude Fe^{3+} in our fits. The dominant M2 site contributes 92% ($\pm 2\%$) of the spectral weight resulting in the following chemical formula for the studied orthoenstatite $(\text{M1})(\text{M2})\text{Si}_2\text{O}_6$: $(\text{Mg}_{0.980}\text{Fe}_{0.020(\pm 0.005)})$ $(\text{Mg}_{0.760}\text{Fe}_{0.240})\text{Si}_2\text{O}_6$. The relative weights of the two sites were fixed to the ambient pressure values for the high-pressure fits. The fitting results we obtained at ambient pressure agree very well with results from previous studies using conventional Mössbauer spectroscopy on a sample from the same run charge (Jackson et al. 2009) and on samples with similar composition and structure (e.g., Pasternak et al. 1992; Dyar et al. 2007; Wang et al. 2005) (Table 1a). The high degree of Fe^{2+} ordering observed in our sample using both conventional and synchrotron Mössbauer spectroscopic methods (Jackson et al. 2009; this study) is likely due to a relatively slow cooling rate experienced during the quench of our sample (e.g., Domeneghetti and Steffen 1992; Wang et al. 2005; Dyar et al. 2007) and is more comparable to natural orthopyroxenes (Wang et al. 2005; Nestola et al. 2008).

TABLE 1A. Comparison with previous conventional Mössbauer spectroscopy measurements of $(\text{Mg,Fe})_2\text{Si}_2\text{O}_6$ orthopyroxene at ambient temperature and pressure.

	Method	Fe/(Fe + Mg)	M1 IS (mm/s)	M1 QS (mm/s)	M2 IS (mm/s)	M2 QS (mm/s)	Fe^{2+} M1 (wt%)
This study	SMS	0.13*	1.191(4)	2.46(5)	1.151(4)	2.22(5)	8(2)
Jackson et al. 2009	MB	0.13*	1.19(1)	2.55(2)	1.16(1)	2.17(1)	8(2)
Pasternak et al. 1992	MB	0.10†	1.179(2)	2.51(1)	1.147(2)	2.22(2)	NR
Dyar et al. 2007	MB	0.10‡	1.16	2.55	1.14	2.09	15
		0.20§	1.17	2.47	1.15	2.10	16.5
		0.20	1.17	2.50	1.15	2.11	15.5
Wang et al. 2005	MB	0.01#	NR	NR	NR	NR	9.3(3)
		0.16#	NR	NR	NR	NR	5.0(3)

Notes: The differences in various reported M1 weights are likely due to different cooling rates of the sample. Values in parentheses indicate the uncertainty in the last significant digit determined by fits of the data. Fe/(Fe+Mg) is the molar fraction of iron to the total number of cations in the sample. The sum of the relative weights of the M1 and M2 sites are constrained to equal 1. The IS for M1 in the first footnote is determined from the spectrum using stainless steel foil as a reference absorber. SMS = synchrotron Mössbauer spectroscopy, MB = conventional Mössbauer spectroscopy, IS = isomer shift (α -iron reference), QS = quadrupole splitting, and NR = not reported.

* $(\text{Mg}_{0.980}\text{Fe}_{0.020(5)})(\text{Mg}_{0.760}\text{Fe}_{0.240})\text{Si}_2\text{O}_6$.

† Sample synthesized at 1.5 GPa and 900 °C, slow quench.

‡ Sample synthesized at 1 atm and 950–990 °C, rapid quench.

§ Sample synthesized at 1 atm and 970–980 °C, rapid quench.

|| Sample synthesized at 1 atm and 950 °C, rapid quench.

Natural sample.

TABLE 1B. The error correlation matrix for the fitted parameters at ambient pressure (En87-NaCl), as reported by CONUSS

	M1 weight	M1 QS	M2 IS – M1 IS	M2 QS
M1 weight	1	-0.394	0.665	0.308
M1 QS	-0.394	1	-0.131	-0.855
M2 IS – M1 IS	0.665	-0.131	1	-0.071
M2 QS	0.308	-0.855	-0.071	1

Note: The largest correlation occurs between the QS of the two sites, which is not an unusually high correlation.

En87-NaCl

A two-sites model representing the M1 and M2 Fe^{2+} octahedral sites for Fe^{2+} is a satisfactory model to fit the SMS spectra of En87-NaCl throughout the pressures investigated (ambient to 36 GPa). However, at pressures greater than 10 GPa, the SMS spectra are fit equally well using only one site to represent the behavior of iron. We discuss both models below.

Two different sets of hyperfine parameters (IS, QS, and QS distribution) were used to represent the two distinct Fe^{2+} sites. We report the best-fit hyperfine parameters in Table 2a. Representative spectra for En87-NaCl are shown in Figures 1a and 1b with their associated χ^2 values. Within uncertainties, the QS of both M1 and M2 sites increase with pressure up to 9 GPa (Fig. 2). At 10.1 GPa, the QS for the M1 site decreases, while the distribution of the QS for both sites decreases. At $P > 10.1$ GPa, the QS values of the M1 and M2 sites are roughly constant, while the distributions of QS values for the two sites increase and overlap each other (Fig. 2), reflecting ambiguous local chemical environments for the M1 and M2 sites. The large distributions correlate with the increasing uncertainty in pressure (Table 2a).

TABLE 2A. The best-fit parameters for the two-sites model from the SMS time spectra evaluation for En87-NaCl: $(\text{Mg}_{0.980}\text{Fe}_{0.020(5)})/(\text{Mg}_{0.760}\text{Fe}_{0.240})\text{Si}_2\text{O}_6$

Pressure (GPa)	Pressure uncertainty (GPa)	M1 site IS (mm/s)	M1 site QS (mm/s)	M1 site QS distribution (mm/s)	M2 site IS (mm/s)	M2 site QS (mm/s)	M2 site QS distribution (mm/s)
0.0	0.0	1.191(4)	2.46(5)	0.05	1.151(4)	2.22(5)	0.05
1.7	0.2	1.196(5)	2.51(6)	0.06	1.166(5)	2.3(1)	0.12
2.4	0.2	1.22(2)	2.58(6)	0.05	1.17(2)	2.29(7)	0.05
3.0	0.3	1.23(2)	2.49(6)	0.05	1.18(2)	2.3(1)	0.13
4.3	0.4	1.22(2)	2.55(6)	0.05	1.16(2)	2.3(1)	0.12
5.6	0.5	1.19(2)	2.63(9)	0.07	1.15(2)	2.4(1)	0.10
7.4	0.7	1.20(3)	2.63(7)	0.05	1.15(3)	2.4(1)	0.11
9.0	0.8	1.20(2)	2.6(1)	0.08	1.15(2)	2.4(1)	0.13
10.1	0.9	1.14(2)	2.59(6)	0.05	1.16(2)	2.44(7)	0.06
12	1	1.11(1)	2.6(1)	0.08	1.16(1)	2.5(2)	0.12
14	1	1.13(1)	2.72(8)	0.05	1.16(1)	2.5(2)	0.15
17	2	1.15(1)	2.6(1)	0.08	1.16(1)	2.5(2)	0.16
19	2	1.15(2)	2.7(1)	0.05	1.15(2)	2.5(2)	0.13
22	2	1.18(2)	2.7(1)	0.05	1.13(2)	2.4(3)	0.17
26	2	1.12(2)	2.6(1)	0.05	1.12(2)	2.4(3)	0.19
31	3	1.15(3)	2.6(1)	0.05	1.11(3)	2.4(3)	0.19
36	4	1.11(1)	2.6(2)	0.08	1.12(1)	2.4(3)	0.21

Notes: QS = quadrupole splitting, IS = isomer shift (α -iron reference). The uncertainties are given in parenthesis at the 90% confidence level for the last reported significant digit.

TABLE 2B. The best-fit parameters for the one-site model from the SMS time spectra evaluation for En87-NaCl: $(\text{Mg}_{0.980}\text{Fe}_{0.020(5)})/(\text{Mg}_{0.760}\text{Fe}_{0.240})\text{Si}_2\text{O}_6$

Pressure (GPa)	Pressure uncertainty (GPa)	IS (mm/s)	QS (mm/s)	QS distribution (mm/s)
10.1	0.9	1.16(2)	2.5(2)	0.14
12	1	1.16(1)	2.5(2)	0.22
14	1	1.16(1)	2.5(3)	0.30
17	2	1.16(1)	2.5(3)	0.30
19	2	1.15(2)	2.5(3)	0.25
22	2	1.13(2)	2.5(3)	0.21
26	2	1.12(2)	2.5(3)	0.21
31	3	1.11(3)	2.4(3)	0.15
36	4	1.08(1)	2.4(3)	0.17

Notes: Refer to Table 2a.

TABLE 2C. The best-fit parameters for the two-sites model from the SMS time spectra evaluation for En87-Ne: $(\text{Mg}_{0.980}\text{Fe}_{0.020(5)})/(\text{Mg}_{0.760}\text{Fe}_{0.240})\text{Si}_2\text{O}_6$

Pressure (GPa)	Pressure uncertainty (GPa)	M1 site IS (mm/s)	M1 site QS (mm/s)	M2 site IS (mm/s)	M2 site QS (mm/s)
4.1	0.2	1.10(3)	2.90(8)	1.09(3)	2.25(6)
5.8	0.4	1.11(1)	2.86(7)	1.07(1)	2.27(6)
7.7	0.5	1.10(1)	2.91(7)	1.08(1)	2.29(6)
9.3	0.5	1.13(1)	2.92(7)	1.08(1)	2.32(6)
10.1	0.4	1.13(1)	2.90(8)	1.07(1)	2.33(6)
12.8	0.5	1.11(1)	2.94(7)	1.08(1)	2.28(6)
14.7	0.7	1.11(1)	2.93(7)	1.08(1)	2.29(6)
16.4	0.6	1.11(1)	2.96(7)	1.08(1)	2.31(6)
17.5	0.6	1.11(1)	2.96(7)	1.08(1)	2.32(6)
18.8	0.7	1.11(1)	2.96(7)	1.07(1)	2.33(6)
19.9	0.7	1.10(2)	2.93(8)	1.07(2)	2.33(6)
21.5	0.8	1.08(2)	2.98(8)	1.06(2)	2.35(6)
23.4	0.8	1.08(2)	2.98(8)	1.06(2)	2.35(6)
24.2	0.9	1.10(2)	2.92(8)	1.06(2)	2.34(6)
25.0	0.9	1.08(2)	2.96(8)	1.07(2)	2.35(6)
26.8	0.9	1.10(1)	2.88(7)	1.06(1)	2.34(6)

Notes: Refer to Table 2a.

Therefore, local structural variations corresponding to a phase transition could be inferred to occur at ~ 10 GPa.

A slight change in trend for the IS values of both M1 and M2 sites is observed around 3 GPa (Fig. 2b; Table 2a). This behavior may be due to the start of silicate tetrahedra compression by Si-O bond shortening between ~ 4 and ~ 9 GPa (Angel and Hugh-Jones 1994; Hugh-Jones et al. 1997; Taran and Langer 2003). The IS of both M1 and M2 sites show relatively small variations with

increasing pressure. At $P > 10$ GPa, the IS values of the M1 and M2 sites fluctuate around a common value of ~ 1.15 mm/s. Such a behavior indicates that the s-electron densities in the Fe nuclear position of both M1 and M2 sites become indistinguishable. With the above behavior of IS and QS values at $P > 10$ GPa, it makes sense to reduce the fitting parameters to a one-site model (i.e., $M1 = M2$).

We applied the one-site model to the data sets at all pressures and examined its validity. The physical assumption of this model is that when the M1 and M2 sites appear indistinguishable, one can allocate one set of hyperfine parameters with a broad QS distribution. In comparison with the two-sites model, the one-site model does not provide adequate fits to the data below 10 GPa, as indicated by the relatively high fitting χ^2 . For $P > 10$ GPa, the fitting χ^2 of the one-site model is comparable or even slightly smaller than the two-sites model (Fig. 1b). For $P > 10$ GPa, the QS and IS values for one iron site are approximately the site-occupancy weighted average of the two distinct sites with small negative fitting slopes as a function of pressure (Fig. 2). The distribution of the QS in the one-site model is large, a finding that is consistent with our results assuming two sites.

En87-Ne

In the experiments with the cell loaded with Ne as a pressure medium, the two-sites model representing the M1 and M2 Fe^{2+} octahedral sites provides the best fit to the SMS spectra at all pressures investigated (4.1 to 26.8 GPa) (Table 2c, Fig. 1c). A one-site model was tested on the En87-Ne data set and resulted in non-physical fitting results. It is worth mentioning that the fitted distribution of QS values was always quite small (less than 0.02 mm/s), so we fixed this value to 0.02 mm/s.

The QS for the M1 site is not sensitive to pressure increase and therefore indicates that the local distortion of the M1 site is small at all pressures investigated here. Results from single-crystal X-ray diffraction studies on $(\text{Mg,Fe})_2\text{Si}_2\text{O}_6$ pyroxene show that the changes in the bond lengths, octahedron volume, and distortion of the M1 site remain small from 4.7 GPa to their highest pressure investigated, 7.5 GPa (Hugh-Jones et al. 1994, 1997). The QS of the M2 site increases with increasing

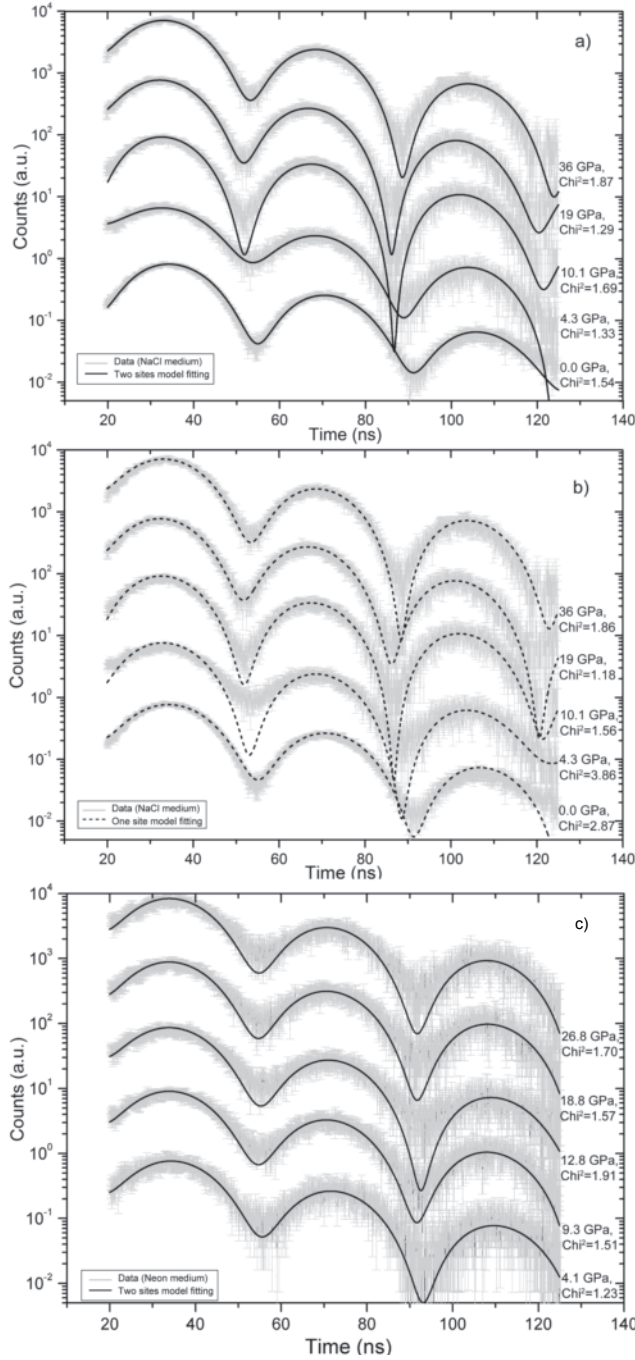


FIGURE 1. Representative SMS time spectra (gray) for En87-NaCl and En87-Ne at different pressures with best-fit parameters associated with the fitting models provided in Table 2. **(a)** En87-NaCl: best-fit two-sites model (black solid lines). **(b)** En87-NaCl: best-fit one-site model (black dashed lines). We find that the one-site model fitting is not convincing below 10.1 GPa for En87-NaCl. **(c)** En87-Ne: best-fit two-sites model. For the lowest spectrum in each panel, the actual collected number of events or counts is normalized to one. The other spectra are of similar statistical quality and have been offset by an order of magnitude for clarity. The pressure and fitting χ^2 are adjacent to each spectrum. The Poisson standard deviation is the uncertainty in counts and shown as vertical bars for each data point.

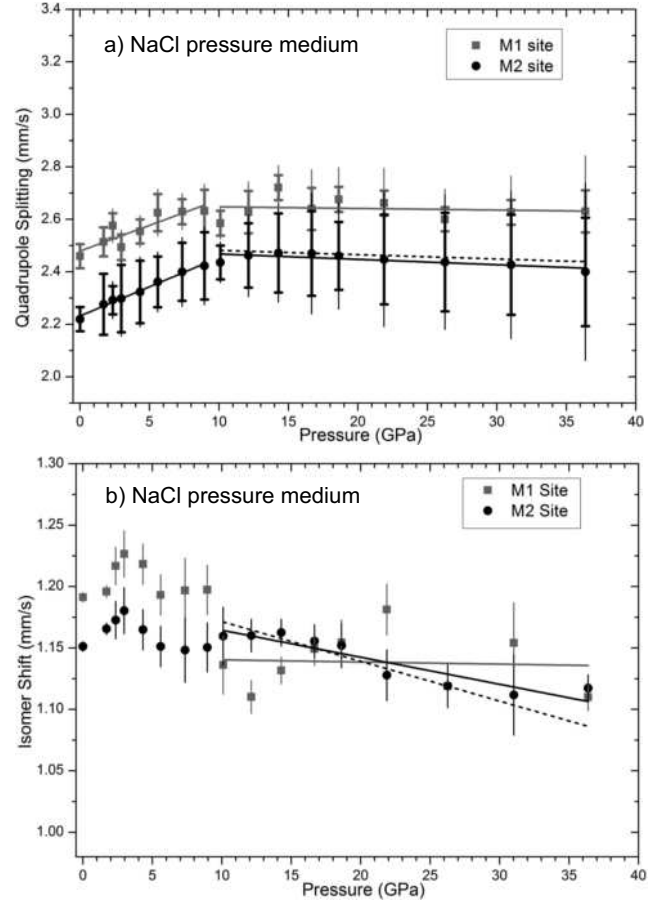


FIGURE 2. The best-fit hyperfine parameters derived from the time spectra of En87-NaCl assuming two distinct iron sites (M1 and M2) (Table 2a). **(a)** Quadrupole splitting (QS) as a function of pressure, where the thick bars denote the distribution of QS and the thin bars are the fitting errors. **(b)** Isomer shift as a function of pressure. Note that the hyperfine parameters from the one-site model (Table 2b) are not shown for clarity. The least-squares regression lines are guides to the eye for a sub-set of the data: two-sites model (solid lines) and one-site model (dashed line). Gray symbols are values and linear fits for the M1 site, and black symbols are the values and linear fits for the M2 site.

pressure up to 10.1 GPa. At 12.8 GPa, the value drops to 2.28 ± 0.05 mm/s, then continues to increase to 26.8 GPa (Fig. 3). At $P > 12.8$ GPa, the QS values of both sites increase at a lower rate than that observed in the lower pressure region. This may indicate a higher resistance to compression in the high-pressure phase, if the observed changes in hyperfine fields between 10.1 and 12.8 GPa are related to a structural transition.

With the exception of the M1 site at pressures lower than 10.1 GPa, the IS decreases with increasing pressure, which indicates an increase of s-electron density likely due to compression. The change of sign in the IS trend with pressure at $P > 10.1$ GPa might be related to a local structural change.

DISCUSSION AND CONCLUSIONS

Influence of different pressure media

We carried out two independent SMS experiments, where the major difference was the pressure medium used. A softer pressure

medium can provide a more hydrostatic environment, whereas a harder pressure medium may accumulate a non-hydrostatic component (You et al. 2009). The degree of non-hydrostatic stress is difficult to measure directly. The shear modulus of the pressure medium serves as a relative indicator of the degree of non-hydrostaticity of the pressure medium. Neon has a shear modulus of 7.2 GPa at 6 GPa pressure (Shimizu et al. 2005), whereas the shear modulus of NaCl at same pressure is 22.8 GPa (Bartels and Schuele 1965). In our experiments, we infer the deviation of pressures within the sample chamber to be proportional to the degree of non-hydrostaticity (Iizuka et al. 2010). The pressure uncertainties for the cell loaded with NaCl are higher than those for the sample loaded with Ne (columns in Tables 2a–2c), suggesting that the NaCl pressure medium produces a larger non-hydrostatic stress environment than the Ne medium, an observation consistent with previous studies (e.g., You et al. 2009). In each experiment, we observe an obvious change in trend or discontinuity in one or more hyperfine parameters around 10 GPa. The major differences between the two experiments are some of the pressure-derivatives of the hyperfine parameters and the observed distribution of QS. The distribution of QS in the NaCl experiment is much larger than that in the Ne experiment. Such an observation implies that, in the case of pyroxene, a broad variation in the local chemical environment is not inherent to pyroxene, but rather due to the sample environment.

Local structure variations in orthopyroxene at high pressures

The isomer shift (IS) is determined by the s-electron density near the ^{57}Fe nuclei. The primary factors influencing the IS are (1) the valence number of the Fe cation and (2) octahedron volume (e.g., McCammon and Tennant 1996; Eeckhout et al. 2000). If the valence number of Fe cation changes from divalent to trivalent, the IS would decrease from ~ 1 to ~ 0.5 mm/s (Eeckhout et al. 2000). In our study, the IS values for both sites are all around 1 mm/s (Table 2). Therefore, the dominant valence number for the Fe cation in this study is divalent (+2). The IS for most sites decrease with pressure, and is likely due to the anticorrelation between s-electron density and the IS value (McCammon and Tennant 1996).

The quadrupole splitting (QS) is strongly related to the non-cubic distortion in the Fe^{2+} -containing octahedral sites in our experimental context. There are also two components for QS: the valence term that comes from the spatial extension of valence electron clouds, and the lattice term that demonstrates the influence of the nearby ions in the crystal lattice. The valence term will increase with increasing deviation from the initial polyhedral shape, and finally keeps at a maximum value; while the lattice term will continuously but slowly decrease with increasing deviation from the initial polyhedral shape (Ingalls 1964; Lin et al. 1993; McCammon and Tennant 1996; Eeckhout et al. 2000). For the cell loaded with NaCl as pressure medium and at pressures below 10 GPa, the QS of both M1 and M2 sites increase with pressure. This is likely due to the increase of the dominant valence term, which comes from the increase in deviations from the initial polyhedral shape with compression. At 10.1 GPa, the QS of the M1 site drops relative to the low- and high-pressure trends. At pressures larger than 10 GPa, the linear fitting slopes

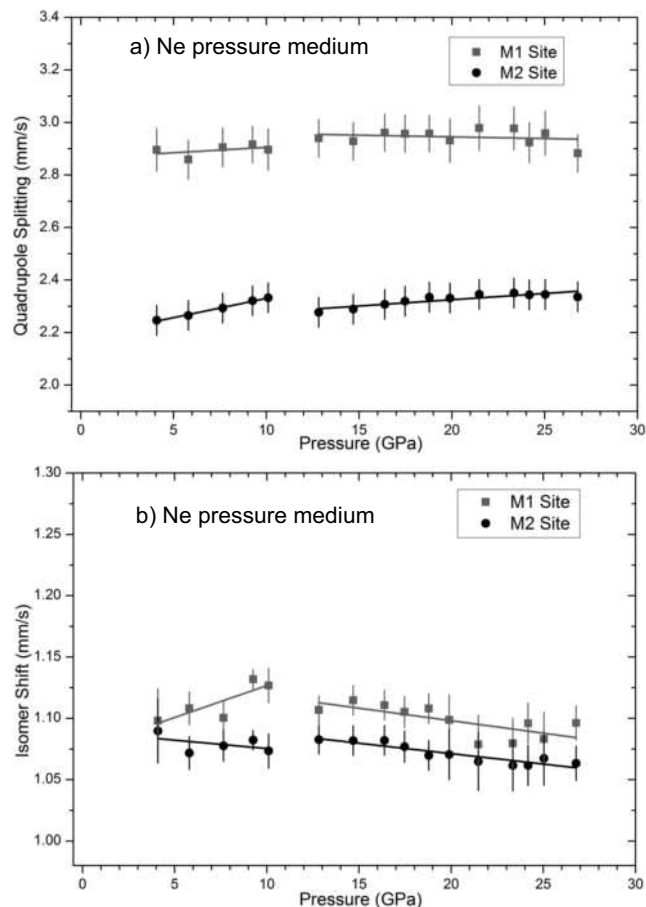


FIGURE 3. The best-fit hyperfine parameters derived from the time spectra of En87-Ne (Table 2c). (a) Quadrupole splitting (QS) as a function of pressure, where the thin bars are the fitting errors. The distribution of QS is fixed to 0.02 mm/s. (b) Isomer shift as a function of pressure. The symbols have the same meaning as stated in Figure 2.

of QS of both sites change from positive to slightly negative values, indicating that the valence term reached the maximum value and that the change of lattice term dominates.

The most obvious feature in the QS measurement in the En87-Ne is one abrupt drop of M2 site QS, detected between 10.1 and 12.8 GPa, indicating a structural transition may be occurring. We found that the M1 QS in En87-Ne is higher than in En87-NaCl. According to previous single-crystal diffraction study using DAC with quasihydrostatic methanol-ethanol solution as pressure medium, the M1 octahedron is mostly compressed below 4.76 GPa (volume shrinks from 11.92 \AA^3 in room pressure to 11.47 \AA^3 at 4.76 GPa), and from 4.76 to 7.50 GPa the volume of the M1 octahedron keeps nearly constant around 11.46 \AA^3 (Hugh-Jones et al. 1997). Therefore, we interpret the higher M1 QS values in En87-Ne as a result of a complete compression of M1 octahedron, which leads to a smaller M1 octahedron volume, a larger electron density to decrease the IS, and a larger valence contribution to raise the QS. Based on single-crystal XRD studies up to 7.5 GPa, the M2 octahedron distorts more quickly than the M1 octahedron (Hugh-Jones et al. 1997). This observation could explain why the QS of the M2 site increases faster than the M1 site in both experiments (Figs. 2 and 3). One recent

theoretical simulation also reveals that the M1 site will remain unchanged during select displacive transitions (Jahn 2008). If these displacive transitions are the origin of the abrupt jump of the hyperfine parameters in En87-Ne, then it can explain why the QS of M1 site has a much smaller change than the QS of M2 site during this transition.

Based on the changes in values and trends of the QS around 10 GPa, there may be a structural transition occurring. The candidates for this transition include *Pbca-Cmca* or *Pbca-Ibca* displacive transitions (Jackson et al. 2004), *Pbca-P2₁ca* or *Pbca-Pbca* displacive transitions (Jahn 2008) or *Pbca-C2/c* reconstructive transition (Kirby and Stern 1993; Hugh-Jones et al. 1996, 1997; Kung et al. 2004; Akashi et al. 2009). The *P2₁ca* phase and isosymmetric *Pbca* phase haven't been directly observed in experiments. One would need X-ray diffraction data on this sample or on a sample with similar composition in this pressure range. The pressure range in which we observe a discontinuity in some hyperfine parameters (10.1 to 12.8 GPa) matches with changes observed in an ultrasonics study (13 to 14 GPa) (Kung et al. 2004), a Raman spectroscopic study (10 to 11 GPa) (Lin 2003), and an X-ray diffraction study (10.4 GPa) (Lin et al. 2005) using Mg₂Si₂O₆ orthoenstatite as starting material (Fig. 4). Our observations are also reasonably consistent

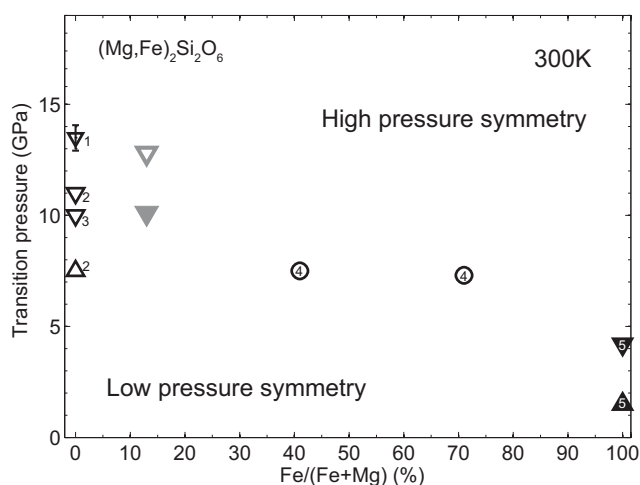


FIGURE 4. High-pressure observations and reported transition pressures from experiments using orthopyroxene with different Fe/(Fe+Mg) ratios as the starting material at 300 K. Each triangle indicates a specific reported phase transition pressure. In studies where the pressure was not high enough to observe a transition, we note where the highest pressure *Pbca* was observed with an open circle. Reverse triangles are transitioning pressures observed on compression, and normal triangles are transition pressures observed on decompression. For the iron-poor studies, the low-pressure starting symmetry is *Pbca* and the high-pressure symmetry has not been determined. For orthoferrosilite, the low-pressure starting symmetry is *Pbca* and the high-pressure symmetry is *C2/c*; on decompression, the low-pressure symmetry was found to be *P2₁/c*. We plot and list the following results (method, pressure-transmitting medium), 1 = Kung et al. 2004 (XRD+ultrasonics, NaCl); 2 = Lin 2003 (Raman, deionized water); 3 = Lin et al. 2005 (XRD, deionized water); 4 = Hugh-Jones and Angel 1997 (XRD, 4:1 methanol:ethanol solution) 5 = Hugh-Jones et al. 1996 (XRD, 4:1 methanol:ethanol solution); open gray triangle: this study (SMS, Ne); solid gray triangle: this study (SMS, NaCl).

with atomistic simulations that predict metastable transitions in *Pbca*-structured orthoenstatite to *P2₁ca* (9 GPa) or a different *Pbca* phase (14 GPa) (Jahn 2008).

ACKNOWLEDGMENTS

We thank E.A. Hamecher, C.A. Murphy, and J.K. Wicks for help in conducting experiments, Y. Fei for synthesizing the sample, and the following for support: NSF-EAR-0711542, CAREER EAR-0956166, and Caltech. Use of the Advanced Photon Source was supported by the U.S. D.O.E., O.S., O.B.E.S. (DE-AC02-06CH11357). Sector 3 operations and the gas-loading system at GSE-CARS are supported in part by COMPRES under NSF Cooperative Agreement EAR 06-49658. Use of HPCAT is supported by DOE-BES, DOE-NNSA, NSF, and the W.M. Keck Foundation. We thank Jennifer Kung for handling our manuscript and an anonymous reviewer for helpful comments.

REFERENCES CITED

- Akashi, A., Nishihara, Y., Takahashi, E., Nakajima, Y., Tange, Y., and Funakoshi, K. (2009) Orthoenstatite/clinoenstatite phase transformation in MgSiO₃ at high pressure and high temperature determined by in situ X ray diffraction: Implications for nature of the X discontinuity. *Journal of Geophysical Research-Solid Earth*, 114, B04206.
- Anderson, D.L. (2007) *New Theory of the Earth XV*, 384 p. Cambridge University Press, U.K.
- Angel, R.J. and Hugh-Jones, D.A. (1994) Equations of state and thermodynamic properties of enstatite pyroxenes. *Journal of Geophysical Research-Solid Earth*, 99, 19777–19783.
- Bartels, R.A. and Schuele, D.E. (1965) Pressure derivatives of elastic constants of NaCl and KCl at 295 degrees K and 195 degrees K. *Journal of Physics and Chemistry of Solids*, 26, 537–549.
- Cameron, M. and Papike, J.J. (1981) Structural and chemical variations in pyroxenes. *American Mineralogist*, 66, 1–50.
- Catalli, K., Shim, S.H., Prakapenka, V.B., Zhao, J.Y., Sturhahn, W., Chow, P., Xiao, Y.M., Liu, H.Z., Cynn, H., and Evans, W.J. (2010) Spin state of ferric iron in MgSiO₃ perovskite and its effect on elastic properties. *Earth and Planetary Science Letters*, 289, 68–75.
- Deuss, A. and Woodhouse, J.H. (2002) A systematic search for mantle discontinuities using SS-precursors. *Geophysical Research Letters*, 29, 1249–1252.
- Domeneghetti, M.C. and Steffen, G. (1992) M1, M2 site populations and distortion parameters in synthetic Mg-Fe orthopyroxenes from Mössbauer spectra and X-ray structure refinements. *Physics and Chemistry of Minerals*, 19, 298–306.
- Dyar, M.D., Klima, R.L., Lindsley, D., and Pieters, C.M. (2007) Effects of differential recoil-free fraction on ordering and site occupancies in Mössbauer spectroscopy of orthopyroxenes. *American Mineralogist*, 92, 424–428.
- Eeckhout, S., De Grave, E., McCammon, C., and Vochten, R. (2000) Temperature dependence of the hyperfine parameters of synthetic *P2₁/c* Mg-Fe clinopyroxenes along the MgSiO₃-FeSiO₃ join. *American Mineralogist*, 85, 943–952.
- Grocholski, B., Shim, S.H., Sturhahn, W., Zhao, J., Xiao, Y., and Chow, P.C. (2009) Spin and valence states of iron in (Mg_{0.8}Fe_{0.2})SiO₃ perovskite. *Geophysical Research Letters*, 36, L24303.
- Hugh-Jones, D.A. and Angel, R.J. (1997) Effect of Ca²⁺ and Fe²⁺ on the equation of state of MgSiO₃ orthopyroxene. *Journal of Geophysical Research-Solid Earth*, 102, 12333–12340.
- Hugh-Jones, D., Chopelas, A., and Angel, R. (1997) Tetrahedral compression in (Mg,Fe)SiO₃ orthopyroxenes. *Physics and Chemistry of Minerals*, 24, 301–310.
- Hugh-Jones, D., Sharp, T., Angel, R., and Woodland, A. (1996) The transition of orthoferrosilite to high-pressure *C2/c* clinoferrosilite at ambient temperature. *European Journal of Mineralogy*, 8, 1337–1345.
- Hugh-Jones, D.A., Woodland, A.B., and Angel, R.J. (1994) The structure of high-pressure *C2/c* ferrosilite and crystal-chemistry of high-pressure *C2/c* pyroxenes. *American Mineralogist*, 79, 1032–1041.
- Iizuka, R., H. Kagi, and K. Komatsu (2010) Comparing ruby fluorescence spectra at high pressure in between methanol-ethanol pressure transmitting medium and its deuteride. *Journal of Physics: Conference Series*, 215, 012177.
- Ingalls, R. (1964) Electric-field gradient tensor in ferrous compounds. *Physical Review*, 133, 787–795.
- Jackson, J.M., Sinogeikin, S.V., Carpenter, M.A., and Bass, J.D. (2004) Novel phase transition in orthoenstatite. *American Mineralogist*, 89, 239–244.
- Jackson, J.M., Sturhahn, W., Shen, G., Zhao, J., Hu, M., Errandonea, D., Bass, J.D., and Fei, Y. (2005) A synchrotron Mössbauer spectroscopy study of (Mg, Fe) SiO₃ perovskite up to 120 GPa. *American Mineralogist*, 90, 199–205.
- Jackson, J.M., Hamecher, E.A., and Sturhahn, W. (2009) Nuclear resonant X-ray spectroscopy of (Mg, Fe) SiO₃ orthoenstatites. *European Journal of Mineralogy*, 21, 551–560.
- Jahn, S. (2008) High-pressure phase transitions in MgSiO₃ orthoenstatite studied by atomistic computer simulation. *American Mineralogist*, 93, 528–532.
- Kirby, S.H. and Stern, L.A. (1993) Experimental dynamic metamorphism of mineral

- single crystals. *Journal of Structural Geology*, 15, 1223–1240.
- Klima, R.L., Pieters, C.M., and Dyar, M.D. (2007) Spectroscopy of synthetic Mg-Fe pyroxenes I: Spin-allowed and spin-forbidden crystal field bands in the visible and near-infrared. *Meteoritics and Planetary Science*, 42, 235–253.
- Kung, J., Li, B., Uchida, T., Wang, Y., Neuville, D., and Liebermann, R. (2004) In situ measurements of sound velocities and densities across the orthopyroxene high-pressure clinopyroxene transition in MgSiO₃ at high pressure. *Physics of the Earth and Planetary Interiors*, 147, 27–44.
- Kung, J., Li, B.S., and Liebermann, R.C. (2006) Ultrasonic observations of elasticity changes across phase transformations in MgSiO₃ pyroxenes. *Journal of Physics and Chemistry of Solids*, 67, 2051–2055.
- Li, J., Sturhahn, W., Jackson, J.M., Struzhkin, V., Lin, J.F., Zhao, J., Mao, H.K., and Shen, G. (2006) Pressure effect on the electronic structure of iron in (Mg, Fe)(Si, Al)O₃ perovskite: A combined synchrotron Mössbauer and X-ray emission spectroscopy study up to 100 GPa. *Physics and Chemistry of Minerals*, 33, 575–585.
- Lin, C. (2003) Pressure-induced metastable phase transition in orthoenstatite (MgSiO₃) at room temperature: a Raman spectroscopic study. *Journal of Solid State Chemistry*, 174, 403–411.
- Lin, C., Zhang, L., and Hafner, S.S. (1993) Local electronic states of Fe²⁺ ions in orthopyroxene. *American Mineralogist*, 78, 8–15.
- Lin, C., Chao, J., and Lin, C. (2005) Metastable phase transition of orthoenstatite (MgSiO₃) under high pressure. *Solid State Sciences*, 7, 293–297.
- Lin, J., Watson, H., G, V., Alp, E., Prakapenka, V., Dera, P., Struzhkin, V., Kubo, A., Zhao, J., and McCammon, C. (2008) Intermediate-spin ferrous iron in lowermost mantle post-perovskite and perovskite. *Nature Geoscience*, 1, 688–691.
- Mao, H.K., Xu, J., and Bell, P.M. (1986) Calibration of the ruby pressure gauge to 800-kbar under quasi-hydrostatic conditions. *Journal of Geophysical Research-Solid Earth and Planets*, 91, 4673–4676.
- McCammon, C. and Tennant, C. (1996) High-pressure Mössbauer study of synthetic clinoferrrosilite, FeSiO₃. *Mineral Spectroscopy: a Tribute to Roger G. Burns*, 281–288.
- McCammon, C., Kantor, I., Narygina, O., Rouquette, J., Ponkrat, U., Sergueev, I., Mezouar, M., Prakapenka, V., and Dubrovinsky, L. (2008) Stable intermediate-spin ferrous iron in lower-mantle perovskite. *Nature Geoscience*, 1, 684–687.
- Nestola, F., Ballaran, T.B., Balić-Žunić, T., Secco, L., and Dal Negro, A. (2008) The high-pressure behavior of an Al- and Fe-rich natural orthopyroxene. *American Mineralogist*, 93, 644–652.
- Pasternak, M.P., Taylor, R.D., Jeanloz, R., and Bohlen, S.R. (1992) Magnetic-ordering transition in Mg_{0.9}Fe_{0.1}SiO₃ orthopyroxene. *American Mineralogist*, 77, 901–903.
- Reynard, B., Bass, J.D., and Brenizer, J. (2010) High-temperature elastic softening of orthopyroxene and seismic properties of the lithospheric upper mantle. *Geophysical Journal International*, 181, 557–566.
- Ringwood, A.E. (1977) *Composition and Origin of the Earth*. Research School of Earth Sciences, Australian National University, Canberra.
- Rivers, M., Prakapenka, V.B., Kubo, A., Pullins, C., Holl, C.M., and Jacobsen, S.D. (2008) The COMPRES/GSECARS gas-loading system for diamond anvil cells at the Advanced Photon Source. *High Pressure Research*, 28, 273–292.
- Shimizu, H., Imaeda, H., Kume, T., and Sasaki, S. (2005) High-pressure elastic properties of liquid and solid neon to 7 GPa. *Physical Review B*, 71, 014108.
- Sturhahn, W. (2000) CONUSS and PHOENIX: Evaluation of nuclear resonant scattering data. *Hyperfine Interactions*, 125, 149–172.
- (2004) Nuclear resonant spectroscopy. *Journal of Physics-Condensed Matter*, 16, 497–530.
- Sturhahn, W. and Jackson, J.M. (2007) Geophysical applications of nuclear resonant scattering. In E. Ohtani, Ed., *Advances in High-Pressure Mineralogy*, 421, p. 157–174. GSA Special Paper, Boulder, Colorado.
- Taran, M.N. and Langer, K. (2003) Single-crystal high-pressure electronic absorption spectroscopic study of natural orthopyroxenes. *European Journal of Mineralogy*, 15, 689–695.
- Wang, L., Moon, N., Zhang, Y., Dunham, W.R., and Essene, E.J. (2005) Fe-Mg order-disorder in orthopyroxenes. *Geochimica et Cosmochimica Acta*, 69, 5777–5788.
- Woodland, A.B. (1998) The orthorhombic to high-P monoclinic phase transition in Mg-Fe pyroxenes: Can it produce a seismic discontinuity? *Geophysical Research Letters*, 25, 1241–1244.
- Woodland, A. and Angel, R. (1997) Reversal of the orthoferrosilite-high-P clinoferrrosilite transition; a phase diagram for FeSiO₃ and implications for the mineralogy of the Earth's upper mantle. *European Journal of Mineralogy*, 9, 245–254.
- Yang, H.X. and Ghose, S. (1995) High-temperature single-crystal X-ray-diffraction studies of the ortho-proto phase-transition in enstatite, Mg₂Si₂O₆ at 1360 K. *Physics and Chemistry of Minerals*, 22, 300–310.
- You, S.J., Chen, L.C., and Jin, C.Q. (2009) Hydrostaticity of pressure media in diamond anvil cells. *Chinese Physics Letters*, 26, 096202.
- Zhang, L., Stanek, J., Hafner, S.S., Ahsbahs, H., Grunsteudel, H.F., Metge, J., and Ruffer, R. (1999) ⁵⁷Fe nuclear forward scattering of synchrotron radiation in hedenbergite CaFeSi₂O₆ hydrostatic pressures up to 68 GPa. *American Mineralogist*, 84, 447–453.

MANUSCRIPT RECEIVED OCTOBER 14, 2010

MANUSCRIPT ACCEPTED JUNE 17, 2011

MANUSCRIPT HANDLED BY JENNIFER KUNG